Planetary Nebulae: A Universal Toolbox in the Era of Precision Astrophysics
Proceedings IAU Symposium No. 384, 2025
O. De Marco, A. Zijlstra & R. Szczerba, eds.
doi:10.1017/S1743921324000358

Remarkable Chemical Complexity in Planetary Nebulae: A Molecule and Dust Perspective

L. M. Ziurys[1] and D. R. Schmidt[2]

[1]Departments of Chemistry and Astronomy, The University of Arizona, USA

[2]Department of Physics and Astronomy, Franklin & Marshall College, USA

Abstract. Despite model predictions, many planetary nebulae appear to have a relatively rich molecular content. Observational studies of over 30 such objects show the presence of a variety of gas-phase molecules, from simple species such as CN and CS, to more complex organics including H_2CO, HC_3N, c-C_3H_2, and CH_3CN. Other PNe contain fullerenes; carbonaceous and silicate dust features are also found. Molecular abundances also do not appear to vary with nebular age. Remnant material from the asymptotic giant branch appears to undergo chemical processing in the protoplanetary nebula phase and then is frozen out in planetary nebulae. PN ejecta are thus in part molecular in content and may account for the observation of complex molecules in diffuse clouds.

Keywords. stars: planetary nebulae, molecular abundances, dust

1. Planetary Nebulae: A Problem for the "Organic Continuum"

Planetary nebulae (PNe) are the final stage in stellar evolution for most stars (1–8 $M_\odot$) following the Asymptotic Giant Branch (AGB). Significant mass loss on the AGB creates a roughly spherical circumstellar envelope, which, by uncertain processes, evolves into the wide variety of morphologies observed in PNe, from elliptical to bipolar to multipolar (Balick & Frank 2002). The ejected envelope also becomes highly ionized by the strong ultraviolet (UV) radiation field generated by the star as it evolves into a white dwarf. The presence of strong UV emission has led to the belief that only atomic and diatomic species would survive from the molecule-rich AGB envelope because of widespread photodissociation. Models of the chemical evolution of PNe predict orders of magnitude decrease in gas-phase molecular abundances over the nebular lifetime (Redman et al. 2003); for example, the HCN abundance falls by $\sim$ 7 orders of magnitude by 10,000 yrs into the PN lifespan.

About $\sim$ 85% of the material that forms the interstellar medium (ISM) has its origins in ejecta from low and intermediate mass stars through the PN phase (Dorschner & Henning 1995). The predicted widespread destruction of gas-phase molecules in PNe therefore implies that there is a sharp discontinuity in molecular chemistry between the AGB and diffuse clouds. The copious production of carbon-carbon bonds that occurs in C-rich AGB stars associated with the so-called "organic continuum" is disrupted such that molecule formation in diffuse clouds must begin from the atomic level. Yet, observations have shown that diffuse clouds contain far more polyatomic molecules than can be produced in situ in the low density environment present (Snow & McCall 2006). Therefore, an outside source must be supplying diffuse clouds with molecular material, suggesting that

© The Author(s), 2025. Published by Cambridge University Press on behalf of International Astronomical Union. This is an Open Access article, distributed under the terms of the Creative Commons Attribution licence (http://creativecommons.org/licenses/by/4.0/), which permits unrestricted re-use, distribution and reproduction, provided the original article is properly cited.

https://doi.org/10.1017/S1743921324000358 Published online by Cambridge University Press

the molecular content of PNe is more complex than models had predicted. PNe could be seeding diffuse clouds and preserving the organic continuum.

CO has long been known to be present in PNe, as demonstrated by the early surveys of Huggins et al. (2005) and Huggins et al. (1996). More recent observations also showed widespread H_2 in objects such as the Helix and Ring Nebulae and other PNe (Speck et al. 2003; Davis et al. 2003). The presence of other molecules in PNe, in particular polyatomic species, was not well-known. A few objects were observed in CN, HCN and HCO^+ in the millimeter range (Bachiller et al. 1997; Cox et al. 1992), and the very young PN NGC 7027 was investigated in some detail (Zhang et al. 2008). This nebula was found to contain molecules as complex as HC_3N and c-C_3H_2; such findings could be attributed to its age of ∼700 yrs in the PN phase, which agreed with chemical models at some level.

2. Molecular Clues from the Aging Helix Nebula

The mystery of polyatomic molecules in diffuse clouds and the problem of the organic continuum led to further investigations into the molecular content of PNe at millimeter wavelengths. Following on the study of Bachiller et al. (1997), Tenenbaum et al. (2009) found H_2CO, c-C_3H_2 and CCH at the same position in the Helix Nebula where HCN and HCO^+ were detected. In contrast to NGC 7027, the Helix is quite old (∼12,000 years) and the presence of 4-5 atom molecules completely contradicted the models. Subsequent observations of the Helix by Zack & Ziurys (2013) and Zeigler et al. (2013) showed widespread HCO^+ and H_2CO across the ∼ 1000″ source. A complete map of the Helix of the J = 1→0 transition of HCO^+ at 89 GHz using the 12 m telescope of the Arizona Radio Observatory (ARO) demonstrated that the molecule was present throughout the nebula (see Figure 1), except in the inner highly-ionized region traced by He^+ emission. Given the radio beam size of ∼ 1 arcmin, over 270 individual positions were measured to produce this image. These high spectral resolution data helped to show that the Helix Nebula was not a helix, but rather bipolar in structure and shaped like a "barrel" oriented almost along the line-of-sight (Zeigler et al. 2013). Subsequent observations revealed that HCN, HNC, CCH, and c-C_3H_2 also had extended distributions in the Helix (Schmidt & Ziurys 2017a; Schmidt et al. 2018a). Even at its advanced stage of evolution, the Helix is chemically-rich, suggesting that indeed its ejecta may contain significant molecular material.

3. The "Level 1" and "Level 2" Planetary Nebula Surveys of HCN and HCO^+

The molecular detections in the Helix Nebula prompted a mini-survey of HCO^+ and CS in five nebulae that spanned the age range 900–10,000 years: K4-47, NGC 6537 (Red Spider), M2-48, NGC 6720 (Ring), and NGC 6853 (Dumbbell). The J = 1→0 and 3→2 transitions of HCO^+ at 89 and 267 GHz and the J = 2→1, 3→2, and J = 5→4 lines of CS (98, 147, and 245 GHz) were observed using the ARO Submillimeter Telescope (SMT) and 12 m antenna (Edwards et al. 2014).The thrust of this work was to examine the change in molecular abundances of these two species with nebular age. Surprisingly, the abundances did not appear to vary significantly, with $f(CS/H_2) \sim 1–4 \times 10^{-8}$ and $f(HCO^+/H_2) \sim 10^{-8}$ - 10^{-7}. This very suggestive result led to the more extensive surveys of Schmidt & Ziurys (2016), Schmidt & Ziurys (2017a), Schmidt & Ziurys (2017b), and Schmidt et al. (2022), which initially focused on HCO^+ and HCN identifications in over a dozen PNe, using their J = 1→0 and 3→2 transitions at 3 and 1.2 mm, respectively. These objects were chosen on the basis of their strong CO emission as determined previously in the Huggins et al. surveys, and covered a range of morphologies (bipolar, multipolar,

https://doi.org/10.1017/S1743921324000358 Published online by Cambridge University Press

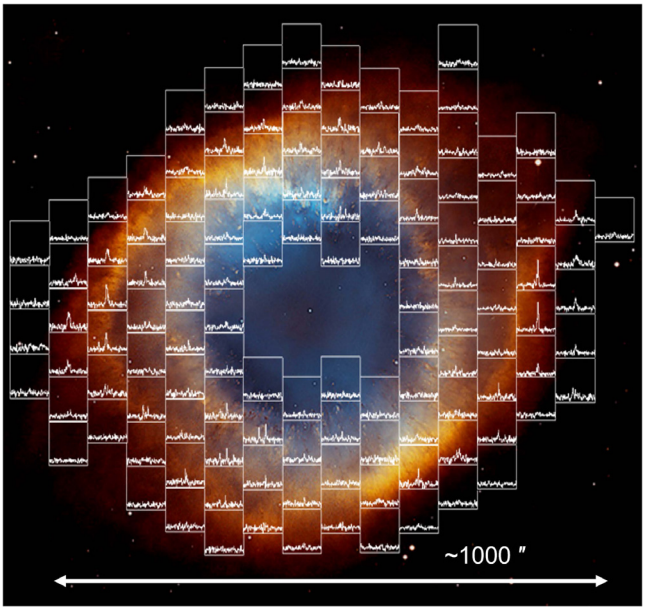

Figure 1. Spectra of the J = 1→0 transition of HCO^+ at 89 GHz observed throughout the Helix Nebula with ∼ 70″ spacings, showing the widespread distribution of this molecule (Zeigler et al. 2013).

elliptical) and ages (900 to 13,000 yrs.) Most of the sample nebulae are displayed in Figure 2.

Measurements were carried out again at ARO, but this time with the new ARO 12 m for the 3 mm work. Of the 17 target PNe in this "Level 1" survey, detections were made of at least one molecule in 13 objects, with sensitivities of a few mK. Fractional abundances found were in the ranges $f(HCO^+/H_2) \sim 0.04–7 \times 10^{-7}$ and $f(HCN/H_2) \sim 0.1–9 \times 10^{-7}$. Radiative transfer modeling, also done in multiple CO transitions, indicated that the molecules were present in warm but quite dense gas, with a typical gas kinetic temperature of $T_K \sim 20–30$ K and $1–5 \times 10^6$ cm^{-3} (Schmidt & Ziurys 2016; Edwards & Ziurys 2013, 2014). The non-detections in certain nebulae may require longer integration times and/or a smaller telescope beam size. Representative Level 1 spectra of the J = 3→2 transition of HCN are presented in Figure 3.

The HCN and HCO^+ detections were subsequently followed by searches for both HNC and CCH in many of the Level 1 objects, as well as the Helix Nebula, as mentioned (Schmidt & Ziurys 2017a,b). These observations were also carried out with the ARO telescopes and focused on the J (or N) = 1→0 and 3→2 transitions at 3 and 1.2 mm. HNC was found in 12 PNe with abundance relative to H_2 of $f \sim 0.02–2 \times 10^{-7}$, resulting in an [HCN]/[HNC] ratio of 1–8. Such low ratios, favoring HNC, are quite different from those found in AGB stars and are important clues to the chemical transformations into the PN phase. CCH was found in the 10 nebulae searched with $f \sim 0.2–47 \times 10^{-7}$, making it one of the more abundant molecules in PNe (Schmidt & Ziurys 2017b; Schmidt et al. 2018a).

The success of the Level 1 studies prompted observations of additional planetary nebulae in HCN and HCO^+, in this case with lower CO intensities, also conducted at ARO at 1 and 3 mm. These so-called "Level 2" sources are shown in Figure 2, and again

https://doi.org/10.1017/S1743921324000358 Published online by Cambridge University Press

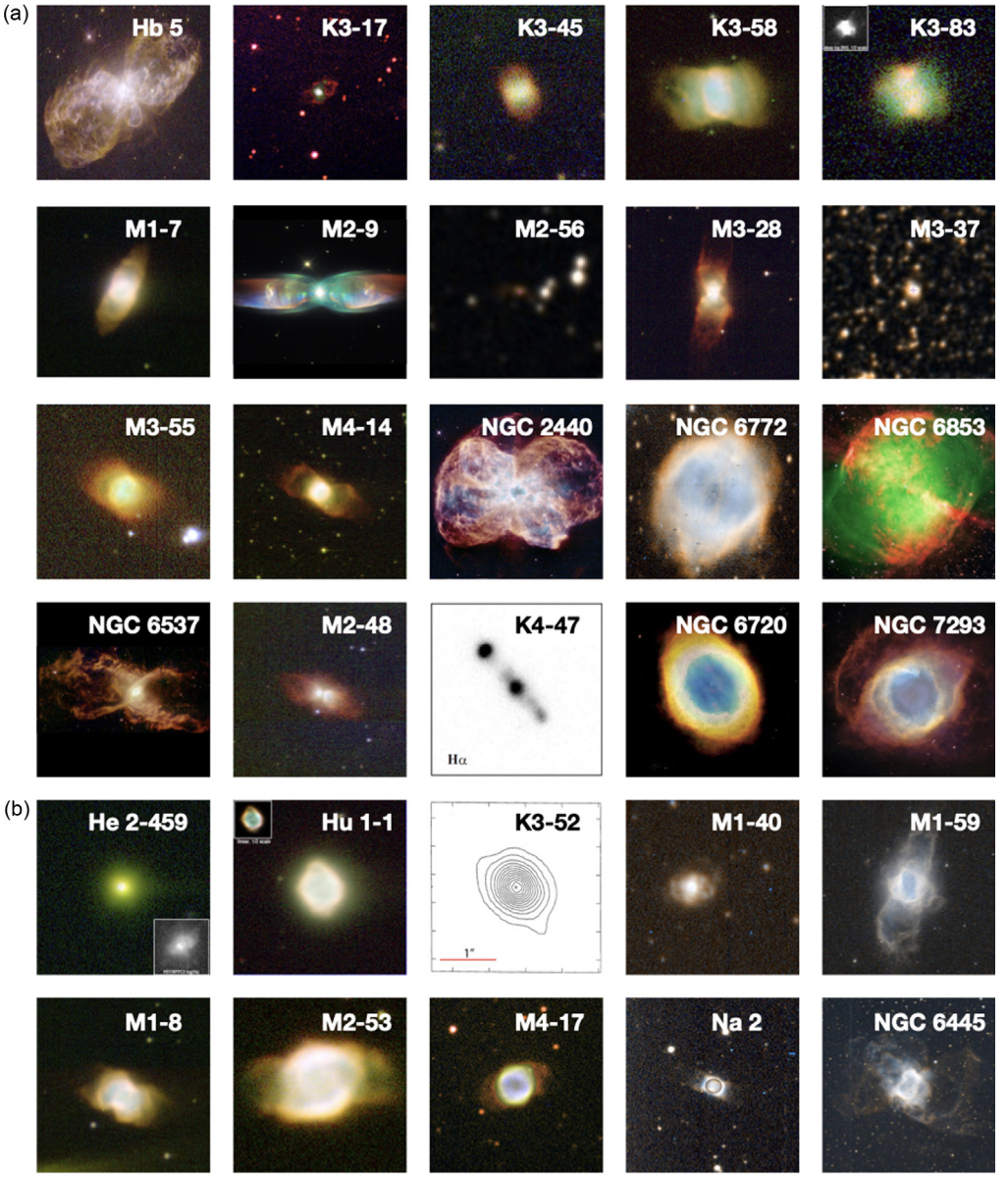

Figure 2. a) PNe from the Level 1 survey and associated studies. b) PNe from the Level 2 survey. All images were acquired from the Planetary Nebula Image Catalog (PNIC) and sources therein, save for M2-9 (source: ESA/Hubble), M2-56 and M3-37 (source: Aladin), NGC 6853 (source: ESO), K4-47 (source: Corradi et al. 2000), and K3-52 (source: Aaquist & Kwok 1990).

represent varied morphologies and ages (Schmidt et al. 2022). Out of the 13 original nebulae, 10 were found to foster at least one of these two polyatomic molecules. A surprising result was the identification of HCO^+ in Na 2, a very old PN estimated to have a kinematic age of ∼28,000 years. The abundances derived were very similar to those of the Level 1 sources, with $f(\mathrm{HCN}) \sim 0.2\text{–}1.5 \times 10^{-7}$ and $f(\mathrm{HCO^+}) \sim 0.3\text{–}5.1 \times 10^{-8}$. The abundances also did not significantly vary with nebular age.

Combined with previous observations, at least 30 PNe contain HCN and/or HCO^+, indicating that polyatomic molecules are common constituents of these objects. The data

https://doi.org/10.1017/S1743921324000358 Published online by Cambridge University Press

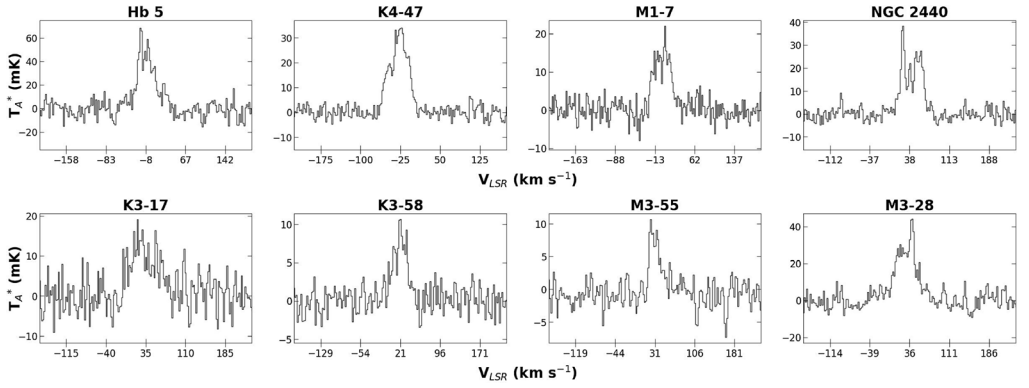

Figure 3. Representative spectra of the J = 3 → 2 line of HCN near 265 GHz observed with the ARO SMT toward several of the "Level 1" PNe (Schmidt & Ziurys 2016).

strongly support a scenario where dense ejecta from PNe seed the interstellar medium with molecular matter.

4. Remarkable Chemical Complexity in Select Planetary Nebulae: K4-47 and M2-48

Some of the Level 1 sources were studied in other molecules. The most chemically-rich PN found to date is the young nebula K4-47 (Schmidt & Ziurys 2019). Measurements at 1, 2, and 3 mm of multiple transitions were carried out at the ARO and Institut de Radioastronomie Millimètrique (IRAM) 30 m telescopes to ensure the accuracy of all molecular identifications. K4-47 is thought to be a young (400–900 yrs), highly collimated, bipolar nebula observed in vibrationally-excited H_2 (Akras et al. 2017). K4-47 was found to contain some unusual species seen in a few other PNe, including HC_3N, N_2H^+, H_2CO, c-C_3H_2, and SiO. However, the more complex molecules CH_3CN, H_2CNH, and CH_3CCH were additionally detected in multiple transitions; see Schmidt & Ziurys (2019) and Figure 4. These species have never before been observed in PNe. In addition, a wide variety of ^{13}C-substituted isotopologues were observed, such as c-^{13}CCCH$_2$, c-CC^{13}CH$_2$, CH$_3{}^{13}$CN, ^{13}CH$_3$CN, CH$_3{}^{13}$CCH, and ^{13}CH$_3$CCH, adding additional evidence for the presence of these complex molecules. Moreover, all three doubly ^{13}C-substituted varieties of HC_3N were identified - the first known object in which all three species have been detected. After CO and H_2, the most abundant molecules in K4-47 were found to be CCH and CN, which have abundances of $f \sim 8 \times 10^{-7}$, relative to molecular hydrogen. Surprisingly, the next most abundant molecule is CH_3CCH, which has $f \sim 6 \times 10^{-7}$. The abundances of CH_3CN and H_2CNH were estimated to be $f \sim 5 \times 10^{-8}$ and $f \sim 10^{-7}$, respectively.

Another PN that was found to have striking properties is M2-48 (Edwards & Ziurys 2014). This object is estimated to be middle-aged at ∼ 4,800 years and has a bipolar morphology and an intricate structure in [N II]. There is a bright, bipolar core, roughly $30'' \times 20''$ in extent, from which the highly collimated bipolar outflow extends, terminating in two symmetric bow-shocked knots, extending $\pm\ 2'$ from the center (López-Martín et al. 2002). H_2 emission has also been detected toward M2-48 by Marquez-Lugo et al. (2013). M2-48 was one of the original sources in the Edwards et al. (2014) survey.

M2-48 was the first PN where SiO and SO_2 were detected; also found were CN, HCN, HNC, CS, SO, HCO^+, N_2H^+, and the isotopologues ^{13}CN, H^{13}CN, HN^{13}C, and H^{13}CO$^+$. A radiative transfer analysis of multiple SiO transitions showed a slightly higher gas kinetic temperature than found in other nebulae, with $T_K \sim 55$ K. SO and SO_2 were

https://doi.org/10.1017/S1743921324000358 Published online by Cambridge University Press

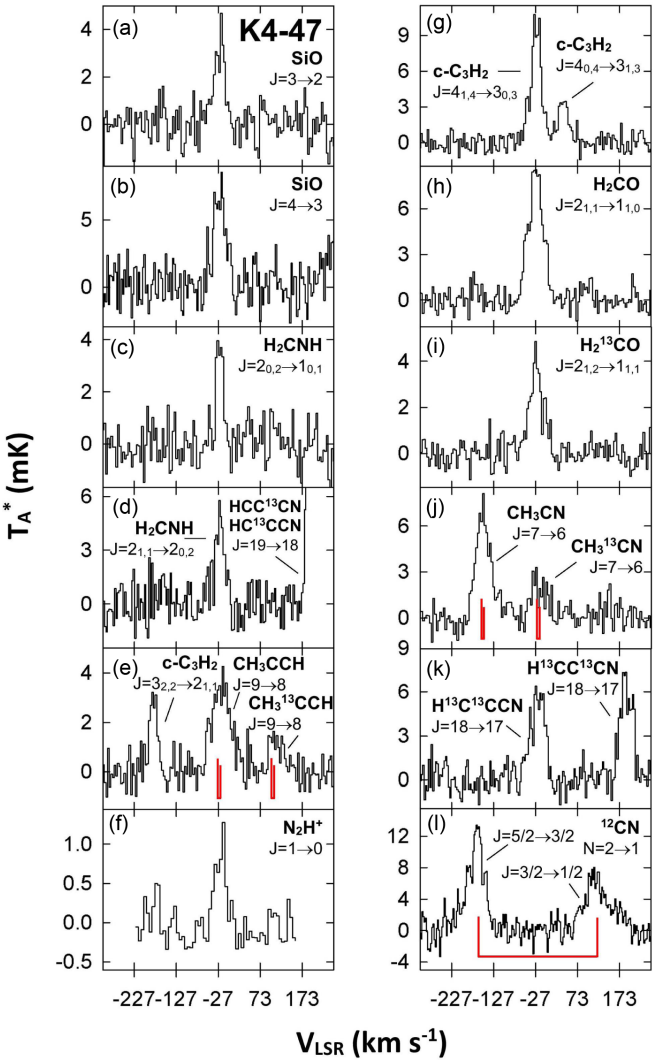

Figure 4. Spectra of unusual and complex molecules found in K4-47, including the organics CH_3CN, H_2CNH, and CH_3CCH (Schmidt & Ziurys 2019).

found to be some of the most prevalent molecules in this nebula, with fractional abundances, relative to H_2, of $f \sim 2.4 \times 10^{-7}$ and 1.2×10^{-7}, indicating an [SO]/[SO_2] ratio of ~ 2. Relatively high ion abundances were measured in M2-48 as well, with $f \sim 10^{-7}$ for both HCO^+ and N_2H^+. An [HCN]/[HNC] ratio of ~ 2 was determined, as typically observed in other PNe. The high abundances of SO and SO_2, along with the presence of SiO with $f \sim 2.9 \times 10^{-8}$, suggest O/C > 1 in this source. Furthermore, the prevalence N_2H^+ indicates possible nitrogen enrichment. Unlike many other PNe, CCH was absent in this nebula, despite extensive searches.

More recent observations by Schmidt et al. have led to the detection of H_2S in M2-48 and a few other PNe. This molecule was identified on the basis of its fundamental transition $J_{Ka,Kc} = 1_{1,0} \rightarrow 1_{0,1}$ which lies at 169 GHz, as shown in Figure 5. A new very

https://doi.org/10.1017/S1743921324000358 Published online by Cambridge University Press

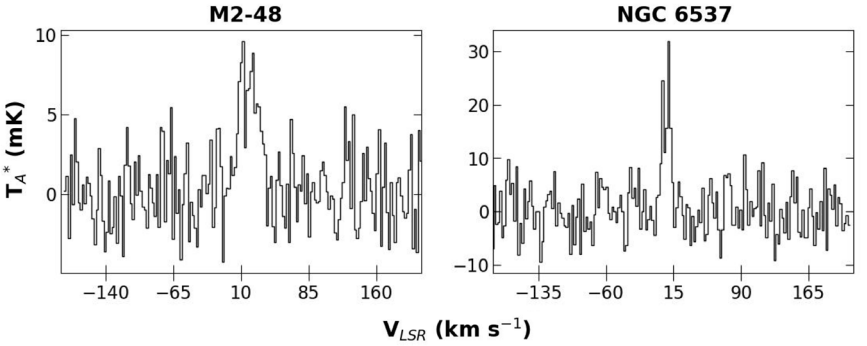

Figure 5. Spectra of the $J_{Ka,Kc} = 1_{1,0} \rightarrow 1_{0,1}$ transition of H_2S near 169 GHz, detected towards the nebulae NGC 6537 and M2-48 (Schmidt et al., in prep.).

sensitive 2 mm receiver built at ARO for the 12 m telescope was used for the measurements. Although the data analysis is preliminary, the presence of H_2S may provide some insight into the so-called "sulfur anomaly" in PNe. A study of O, Ne, S, Cl, and Ar abundances in 85 PNe by Henry et al. (2004), systematically found lower sulfur abundances, relative to H II regions of the same metallicity. This discrepancy has been verified by other observations. Henry et al. suggested that sulfur may be sequestered into grains. However, molecules such as H_2S, SO, and SO_2 may provide an alternative sink.

M2-48 appears to be an O-rich nebula while K4-47 is clearly carbon-rich. The molecular content thus can be used as an indicator of the C/O ratio in PNe. These ratios are likely those from the original AGB stars.

5. Other Nebulae of Interest

The studies of K4-47 and M2-48 are only sampling a small subset of all PNe that have a noteworthy chemistry. Bublitz et al. (2019), for example, has identified interesting molecules such as HCN, CN and HNC in NGC 6853 and NGC 6445. They found a correlation between the [HCN]/[HNC] ratio and UV flux. Further observations of NGC 7027 by the same group has revealed a very complex morphology consisting of multipolar structures actively driven by collimated winds (Moraga Baez et al. 2023). This nebula also contains CH^+ and the rare ion HeH^+ (Neufeld et al. 2020; Güsten et al. 2019).

Several of the Level 2 sources from Schmidt et al. (2022) have also been further investigated for their molecular content. One object of note is NGC 6445, the "Little Gem" Nebula. This PN was initially studied in molecular lines by Bublitz et al. (2019), who identified HCO^+, CN, HCN, and HNC in the nebula in the 3 mm window. Schmidt et al. expanded this data set by measuring the J = 3→2 transitions of HCN and HCO^+, followed by Gold et al. (in prep.) who added CCH, HC_3N, H_2CO, CS, H_2S and c-C_3H_2 to the molecular list. High sensitivity spectra in CO and other molecules suggest that this nebula has four distinct velocity components (Schmidt et al. 2022). The complexity of this structure is currently being unraveled by both ALMA observations (Moraga Baez et al. this volume) and single-dish mapping (Gold et al).

Hu 1-1 is another "Level 2" nebula with some striking properties. Most of the molecule-rich nebulae are bipolar or multipolar in shape, but Hu 1-1 is thought to be elliptical with a binary companion (Weidmann & Gamen 2011). The previous detections of HCN and HCO^+ have been complemented recently by H_2CO, CCH, CN, CS, and c-C_3H_2 (Figure 6; Gold et al. in prep.) These results suggest that morphology may not play a decisive role in the chemistry, but further exploration is clearly needed. Further observations of this

https://doi.org/10.1017/S1743921324000358 Published online by Cambridge University Press

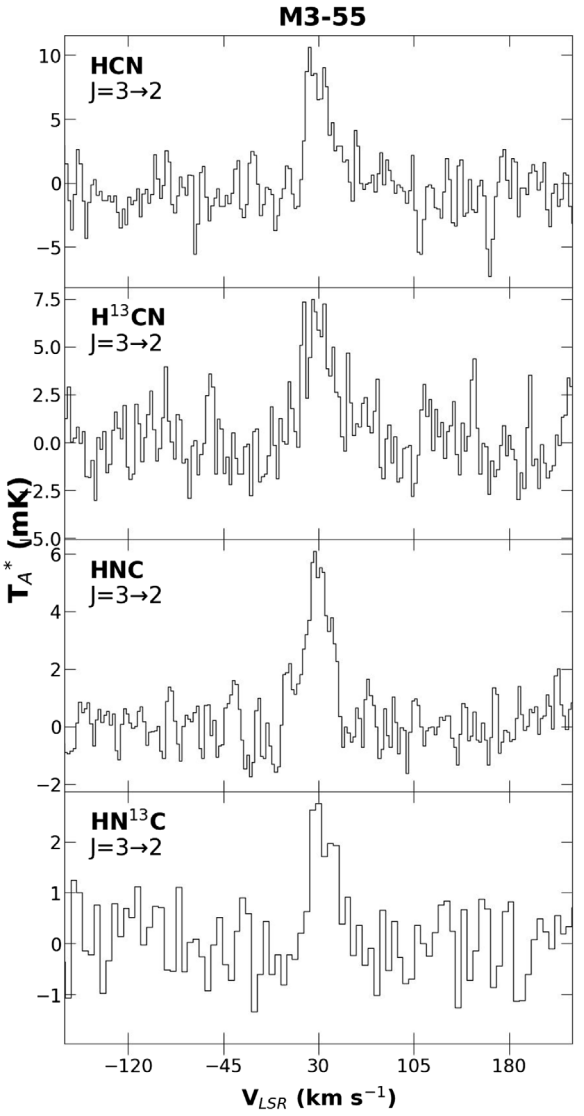

Figure 6. Spectra of molecules observed towards Hu 1-1, an elliptical PN with a binary companion, including H_2CO and c-C_3H_2 (Gold et al. in prep).

rare source are in progress. It is also noteworthy that the spectra from Hu 1-1 have an unusual line profile with a strong central peak combined with a broad, redshifted wing, most visible in CO (Schmidt et al. 2022). This line shape may be related to the binary structure, but high-resolution imaging would give a more complete picture.

6. An Overview of Molecular Abundances in Planetary Nebulae: Beyond CO

The current work has led to the identification of many molecules in PNe, often with multiple transitions (see Table 1 for a complete list). Accurate radiative transfer modeling can then be carried out, establishing not only abundances but densities and temperatures,

https://doi.org/10.1017/S1743921324000358 Published online by Cambridge University Press

Table 1. Molecules Observed in Planetary Nebulae.

H_2	CH^+	HNC	SO_2	CH_2NH
CO	OH	CCH	H_2S	CH_3CN
CO^+	SiO	N_2H^+	H_2CO	CH_3CCH
CN	SO	HCO^+	c-C_3H_2	C_{60}
CS	HCN	HeH^+	HC_3N	C_{70}

as mentioned. Over 30 PNe have now been observed in a variety of species. Although this number is a small subset of the PNe in the Galaxy, it does provide a snapshot of the chemical complexity in these objects. Note that most molecular lines detected in planetary nebulae are quite weak - about 1–20 mK, as shown in Figures 4–6. Many of the PNe observed have a small angular size, such that mm-wave observations are typically "beam-diluted." Systemic studies with long integration times, sensitive receivers, and multiple frequency bands are needed for these detections. Such obstacles have made the study of the molecular content of PNe sporadic until recently. The establishment of a consistent set of molecular abundances in PNe has been a decade-long effort and finally a statistical sample, albeit small, is available.

A summary of molecular abundances measured in PNe for almost all species thus far identified is given in Table 2. The criterion for inclusion in the table is the appearance of a given molecule in at least three nebulae. Therefore, the more complex organics currently unique to K4-47 are not included, but their abundances have been reported in an earlier section. For nebulae with small angular sizes, relative to the mm-wave antenna beam, abundances have been corrected for the source size, based on the optical image. For extended sources, a "clumping" factor is also applied, which compensates for the presence of molecules in knots as opposed to a uniform distribution (see Schmidt & Ziurys 2016). Such clumps are known to exist in the Helix from H_2 observations, for example Meixner et al. (2005). All corrections have been applied to the data in a consistent manner such that meaningful comparisons can be made. Note that when three or more transitions of a given molecule are detected, an estimate of the density and temperature of the gas can be calculated. This situation is common for CO, CS, and larger molecules such as HC_3N. The typical density and temperature range found for the gas in the >30 sample of PNe is $T_k \sim 15$–70 K and $n(H_2) \sim 10^5$-10^7 cm^{-3}. As mentioned, the molecular material is dense but not very hot. These physical properties support the concept that the molecules exist in dense, self-shielding clumps, mixed with dust, embedded in an ionized medium, as theorized decades ago by Howe et al. (1994). Evidence for the "knots" model is apparent in the H_2 observations of sources such as the Helix (e.g. Meixner et al. 2005; Speck et al. 2003). However, contrary to some theoretical predictions (Redman et al. 2003), the clumps apparently do not dissipate on a $t^{-3/2}$ timescale and are more robust than assumed.

As shown in Table 2, CO is the most abundant molecule after (presumably) H_2. The abundance of this molecule is fairly constant across all PNe at $f \sim 10^{-4}$. The next most prevalent species is a polyatomic, CCH, with $f \sim 0.02$–4.7×10^{-6}, with the emphasis on the upper end of the given range. CCH, however, has not been observed in any O-rich PNe. HCN and CN closely follow with $f \sim 0.1$–9×10^{-7} and $f \sim 0.7$–9.9×10^{-7}. These species are abundant in oxygen-rich M2-48 (Edwards & Ziurys 2014) and are also common in O-rich stellar envelopes (Ziurys et al. 2009). HCO^+ is also relatively common, having $f \sim 0.02$–7.4×10^{-7}, with HNC, H_2CO, SO, and c-C_3H_2 equally abundant with $f \sim 0.2$–2×10^{-7}, although HNC has a somewhat lower range. It is also noteworthy that the abundance of HC_3N is as high as $f \sim 10^{-7}$. N_2H^+, SiO, and H_2S (in prep.) are about a factor of 10 lower than the other molecules.

https://doi.org/10.1017/S1743921324000358 Published online by Cambridge University Press

Table 2. Representative Abundances in Planetary Nebulae.

Molecule	f(X/H_2)[a]	References
CO	$\sim 10^{-4}$	-
HCN	0.1–9.1 × 10^{-7}	b, c, d, e, f, g
HCO^+	0.02–7.4 × 10^{-7}	b, c, d, e, g, h, i
CCH	0.02–4.7 × 10^{-6}	b, c, j, k
HNC	0.02–2.2 × 10^{-7}	c, d, f
H_2CO	0.22–2.50 × 10^{-7}	c, i, l
CS	0.05–1.1 × 10^{-7}	c, d, h
CN	0.7–9.9 × 10^{-7}	b, c, d, k, l
SO	0.21–2.40 × 10^{-7}	c, d
SO_2	1.2 × 10^{-7}	d
c-C_3H_2	0.1–1.5 × 10^{-7}	b, k, l
N_2H^+	0.38–9.80 × 10^{-8}	b, c, d, l
SiO	1.4–2.9 × 10^{-8}	d, l
HC_3N	0.09–2.2 × 10^{-7}	b, l

[a] Abundance relative to H_2, [b] Zhang et al. (2008), [c] Edwards & Ziurys (2013), [d] Edwards & Ziurys (2014), [e] Schmidt & Ziurys (2016), [f] Schmidt & Ziurys (2017a), [g] Schmidt et al. (2022), [h] Edwards et al. (2014), [i] Zack & Ziurys (2013), [j] Schmidt & Ziurys (2017b), [k] Schmidt et al. (2018a), [l] Schmidt & Ziurys (2019)

Another important characteristic of the molecular abundances is that they do not appear to vary with the age of the PNe, as mentioned in Section 3 for HCN and HCO^+. This finding is illustrated in Figure 7. Here abundances for HCN, HCO^+, CCH, CS, H_2CO, c-C_3H_2 and N_2H^+ are plotted vs. the age of the nebula host, in circles of varying colors. For a given species, the abundances do not typically vary more than a factor of 10 across 12,000 yrs. For example, the abundance of CCH remains at 10^{-7}-10^{-6}, while the values for H_2CO fluctuate slightly around 10^{-7}. Even more striking is that of HCN, which never drops below 10^{-8} for over 30 PNe. In contrast, the model of Redman et al. (2003) predicts that the abundances of HCN and HCO^+ decrease by factors of 10^6 and 100, respectively. No such decrease is observed. This result strongly supports the idea that PNe seed the diffuse ISM with molecular material, as discussed.

7. The Isotope Mystery

The $^{12}C/^{13}C$ ratio is a sensitive indicator of nucleosynthesis and mixing in the interior of stars (e.g. Abia et al. 2017).^{13}C is an intermediate product of hydrogen-shell burning in the CNO cycle (e.g. Wiescher et al. 2010), produced on the red giant branch (RGB) and brought to the stellar surface in the First, and for more massive stars, Second Dredge-Up. ^{12}C, in contrast, is created by the triple alpha process during helium-burning, which occurs on the AGB and also in supernovae (Herwig 2005). Thermal pulsing on the AGB creates a convective envelope, which, through Third Dredge-Up, brings the ^{12}C to the stellar surface. As a consequence, low $^{12}C/^{13}C$ ratios are expected on the RGB, typically 5–25. The ratios increase on the AGB to > 30, in the process creating carbon stars where C > O (Lebzelter et al. 2019). Overall, observations of $^{12}C/^{13}C$ ratios in evolved stars have supported this picture with lower ratios for oxygen-rich stars, and higher values for carbon-rich objects. For example, in Ramstedt & Olofsson (2014), typical ratios determined for the shells with C < O were $^{12}C/^{13}C \sim$ 5–15, while values of $^{12}C/^{13}C \sim$ 8–46 were found for those with C > O. Milam et al. (2009) found $^{12}C/^{13}C \sim$ 25-90 in C-rich AGB envelopes and substantially lower values of $^{12}C/^{13}C \sim$ 3–35 in oxygen-rich shells.

As molecular observations of PNe were conducted, spectra of ^{13}C-substituted molecules were often observed, enabling a determination of $^{12}C/^{13}C$ ratios. These species include

https://doi.org/10.1017/S1743921324000358 Published online by Cambridge University Press

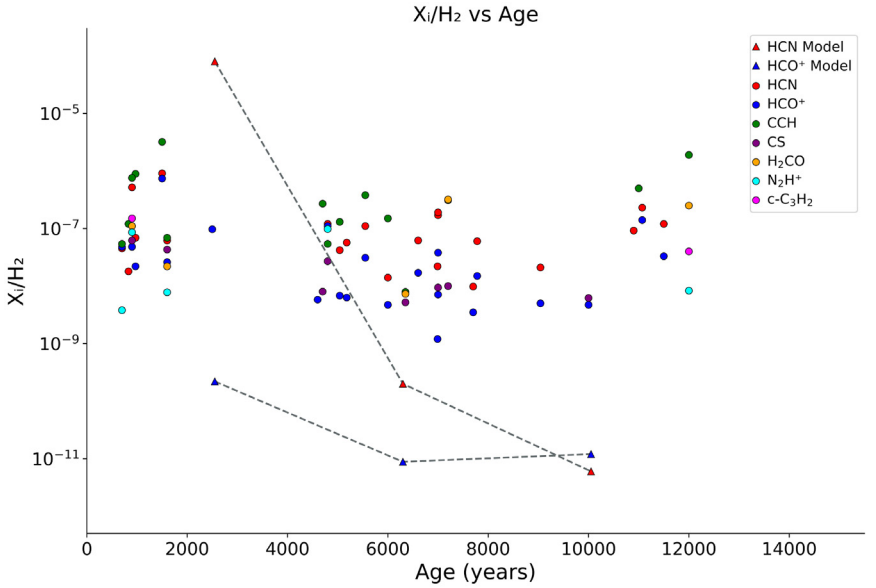

Figure 7. A plot of molecular abundances (circles) for series of PNe vs. their age. Data are shown for HCN, HCO^+, CCH, CS, H_2CO, c-C_3H_2 and N_2H^+. For a given species, the abundances typically do not vary more than a factor of 10 across 12,000 yrs. Theoretical predictions are shown by triangles and dashed lines for HCN and HCO^+, which show orders of magnitude decrease with age, in contrast to the observations.

Table 3. $^{12}C/^{13}C$ Isotope Ratios in PNe [a].

Source	Morphology	Molecular Tracers	$^{12}C/^{13}C$	Previous $^{12}C/^{13}C$ [b]	C/O
NGC 6537	Multipolar	HCN, HNC	2.4–3.5 ± 0.5	-	0.95[c] ≥1[d]
M2-48	Bipolar	HCN, HNC HCO^+, CN	2–4 ±0.6	-	<1[d]
K4-47	Bipolar	CO, CN, HCN, HNC, HCO^+, H_2CO	1.3–3.4 ± 0.6	-	>1[e]
NGC 7293[f]	Bipolar	HCO^+	12.4 ± 5.4	9, 10, 9.4 ± 0.6	0.9–1[g,h] >1[i]
M3-55	Bipolar	HCN, HNC	1.0–1.8 ± 0.8	-	≥1[i]
M3-28	Quadrupolar	HCN	7.2 ± 4.4	-	≥1[i]
M2-9	Bipolar	CO, HCO^+	3.3 ± 1.9 (CO) 13.2 ± 4.9 (HCO^+)	>2	<0.5[j]
NGC 2440	Quadrupolar?	CO, HCN	1.2–1.6 ± 0.7	-	0.5–1.9[h,k]
NGC 6720	Bipolar	HCN, CN	10.8–12.2 ± 4.5	22, 9.5 ± 1.6	1.1[h]
K3-52	Irregular	HCN	1.5 ± 0.5	-	-
K3-70	Elliptical	CO	1.75	-	-
M3-3	Bipolar	HCN	∼ 2.5	∼ 3	-

[a] From Ziurys et al. (2020) except where indicated, [b] From Palla et al. (2000), Balser et al. (2002), Andriantsaralaza et al. (2020); from CO, [c] Pottasch et al. (2000), [d] Edwards et al. (2014), [e] Schmidt et al. (2018b), [f] (+390″, -30″) position, [g] Henry et al. (1999), Henry et al. (2018), [h] Ventura et al. (2017), [i] Based on molecular content, [j] Liu et al. (2001), [k] Bernard-Salas et al. (2002)

https://doi.org/10.1017/S1743921324000358 Published online by Cambridge University Press

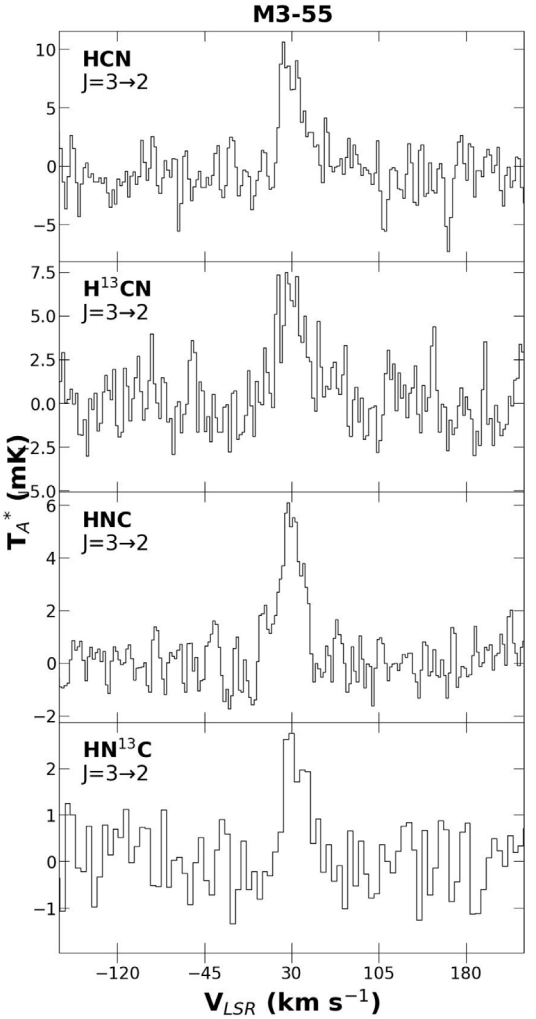

Figure 8. Spectra of the J = 3→2 transition of HCN, $H^{13}CN$, HNC, and $HN^{13}C$ measured toward the PN M3-55. Note the relative strengths of the lines.

CO, HCN, HNC, CN, and others, as previously mentioned for K4-47. Sample spectra are shown in Figure 8, specifically lines of HCN, $H^{13}CN$, HNC, and $HN^{13}C$ in M3-55.

Currently, the ratio has been measured in a sample of 12 PNe, 9 from Ziurys et al. (2020) and new data. These values are summarized in Table 3. The ratios fall in the range 1.0 ± 0.8 to 13.2 ± 4.9. In 7 out of 12 sources, more than one molecule was used in the determination, and often with multiple transitions. Values are very consistent between molecules. It is therefore clear in this sample, many of which are C-rich PNe, that the $^{12}C/^{13}C$ ratios are unexpectedly low - significantly less than in normal carbon stars. Furthermore, in several nebulae, the ratio is < 3.5, the minimum achieved in equilibrium CNO burning (Herwig 2005).

The objects chosen here have ages $\sim$ 900 to 12,000 years and thus sample the entire PN lifespan. However, because nucleosynthesis ceases at the beginning of the PN stage,

https://doi.org/10.1017/S1743921324000358 Published online by Cambridge University Press

age should not play a role in the ratio values. Fractionation is not likely, as Schmidt & Ziurys (2016), Schmidt & Ziurys (2017a), Schmidt & Ziurys (2017b), Zack & Ziurys (2013), Schmidt et al. (2018a), and Edwards et al. (2014) have shown that the molecular gas in PNe is warm, typically 20–50 K. Therefore, the low ratios reflect the end of the AGB.

The lowest isotope ratio that can possibly be produced by equilibrium CNO cycle H-burning is 3.5; yet, for ten nebulae with measured $^{12}C/^{13}C$, the ratio is < 3.5. Non-equilibrium models of abruptly initiated and terminated high temperature proton capture reactions can produce carbon isotope ratios as low as 0.5 (Audouze et al. 1973), commonly accompanied by conversion of C to N. The consistently low $^{12}C/^{13}C$ ratios observed in a dozen PNe, combined with often a high N/O ratio, suggest that a rapid hot process involving proton-capture occurred on the AGB.

8. More Detailed Structure and Chemistry in Planetary Nebulae: ALMA Imaging

Single-dish observations at millimeter wavelengths have clearly demonstrated that molecules are widespread in PNe and can achieve significant complexity. That being said, there is limited information available regarding the spatial distribution of these molecules in the nebulae in which they are found. With few exceptions, the angular sizes of PNe tend to be smaller than the beam size of the single-dish telescopes at the frequencies observed; as a result, it can be determined what molecules are present in these nebulae but not where they reside. Even in cases in which multiple pointings across the PN are possible, there is generally incomplete coverage of the source.

In order to attain the higher spatial resolutions needed to trace the kinematic structure of the molecular outflows, interferometers are needed. Arrays such as SMA and NOEMA have provided such insight. For instance, images of CO^+ and HCO^+ in NGC 7027 made using NOEMA exhibit notably different emission morphologies, with HCO^+ displaced radially outward compared to CO^+ (Bublitz et al. 2023). On the basis of these observations, the authors suggest that the two ions trace different environments, with CO^+ delineating the inner boundaries of the photon-dominated region (PDR) and HCO^+ the signpost of an X-ray dominated region (XDR) surrounding the PDR.

Currently, the most powerful tool to study the distribution of the molecular outflow in PNe is the Atacama Large Millimeter Array (ALMA). One of the earliest objects to be studied with ALMA was the Boomerang Nebula, which was imaged in the CO $J = 1 \rightarrow 0$ and $J = 2 \rightarrow 1$ lines (Sahai et al. 2013). Low angular resolution single dish images suggested a spherical molecular outflow, in contrast to its visible-light morphology. The high resolution ALMA data revealed dense walls of molecular gas surrounding hollow cavities (the bipolar outflow observed in the optical), as well as a compact mass of millimeter-sized grains in the nebula's waist observed through continuum emission. The waist was determined to shape the nebula's illumination, resulting in its hourglass morphology. Subsequent observations of both $J = 1 \rightarrow 0$ and $J = 3 \rightarrow 2$ CO emission provided further insight into the nebula's central waist and bipolar outflow and suggested that it arose from a common-envelope binary interaction (Sahai et al. 2017).

The well-studied Helix Nebula (NGC 7293) has been imaged with ALMA as well. In particular, the C1 globule was observed at the $J = 2 \rightarrow 1$ transitions of ^{12}CO, ^{13}CO, and $C^{18}O$ (Andriantsaralaza et al. 2020). The measurements were used to derive a molecular mass of $\sim 2 \times 10^{-4}$ for the globule, indicating that it may have been previously highly underestimated, along with $^{12}C/^{13}C$ and $^{16}O/^{18}O$ ratios of $\sim$10 and $\sim$115, respectively. Two other globules were observed at 1 mm and 3 mm with ALMA, yielding images of

https://doi.org/10.1017/S1743921324000358 Published online by Cambridge University Press

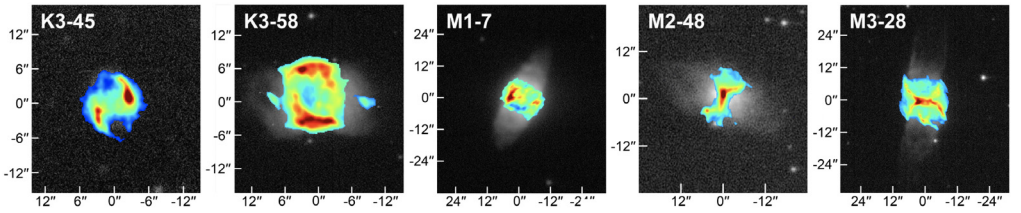

Figure 9. Moment 0 maps of CO J = 2→1 emission in K3-45, K3-58, M1-7, M2-48, and M3-28 overlaid on optical images of the nebula from the PNIC.

^{12}CO, HCN, HCO$^+$, and HNC which revealed their filamentary nature (Bublitz et al. 2020).

Interferometric observations have also been performed on some lesser-known PNe. In particular, five PNe whose molecular composition had been studied to varying degrees using the ARO facilities were recently imaged using ALMA, specifically K3-45, K3-58, M1-7, M2-48, and M3-28 (see Figure 2 for optical images). The nebulae are diverse, covering a range of kinematic ages, from the young (K3-45 at $\sim$ 800 years) to the middle-aged (M1-7 at $\sim$ 6000 years, M2-48 at $\sim$ 5000 years, and M3-28 at $\sim$ 8000 years) to the old (K3-58 at $\sim$ 11,000 years). Further, these PNe exhibit varying morphologies; for instance, K3-45, based on its U-shaped line profiles, is expected to be bipolar, while M3-28 is thought to be quadrupolar.

The ALMA Band 6 receiver in combination with the 12 m array antennas were used to observe the CO J = 2 $\rightarrow$ 1 line in each source, which had been previously identified using the ARO SMT. M1-7, M2-48, and M3-28 were also imaged at the J = 3 $\rightarrow$ 2 lines of HCN and HCO$^+$, which had also been originally measured using the SMT. Given an angular resolution of $\sim$1$''$, the regions of molecular emission were readily resolved in each source. The ALMA datacubes were combined with their single-dish SMT data in order to recover all flux. The resulting CO images are shown in Figure 9.

When overlaid on optical images of the corresponding nebulae, these images demonstrate that the molecular material is generally confined to the central regions of the nebula. This indicates that the molecular material is funneling the bipolar outflows seen in the optical, and suggests that the remnant AGB shell may be transformed into a disk or other structures. Thus, remnant molecular material may play a role in the shaping of PNe.

9. Molecule Survival and the Chemical Transition from the Asymptotic Giant Branch to Planetary Nebulae

The envelopes of AGB stars are resplendent in molecules and set the stage for the formation of PNe. Abundances of molecules in AGB envelopes and PNe do differ substantially. The typical abundance of HCN is $f \sim 10^{-5}$ in C-rich AGB shells, as opposed to $f \sim 10^{-8}$-10^{-7} in observed PNe, most of which also appear to be carbon-rich - a factor of 100–1000 decrease. On the other hand, HCO$^+$ is almost non-existent in C-rich AGB envelopes but has $f \sim 10^{-8}$-10^{-7} in O-rich shells (Pulliam et al. 2011). In PNe, the abundance is $f \sim 0.02$–7.4×10^{-7} and thus far is universally present, despite the C/O ratio of a given nebula. HCO$^+$ therefore is more prevalent in PNe. The abundance of HNC increases dramatically from the AGB to PNe, altering the [HCN]/[HNC] ratios from $>$ 100 to 1–8, as discussed (Schmidt & Ziurys 2017a). In contrast, the CCH abundance drops by no more than a factor of 5, staying relatively constant throughout the AGB-PN transitions (Schmidt & Ziurys 2017b).

https://doi.org/10.1017/S1743921324000358 Published online by Cambridge University Press

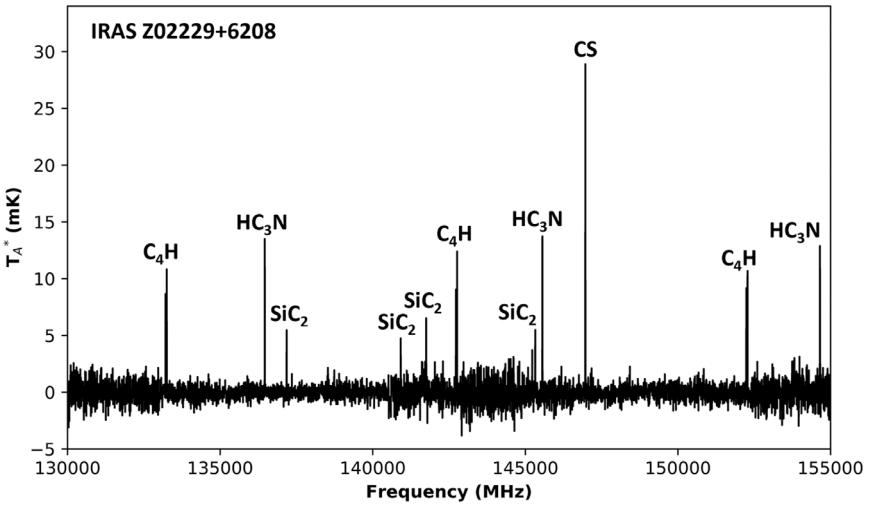

Figure 10. Spectrum of the C-rich PPNe IRAS Z02229+6208 near 145 GHz, showing its diverse chemical composition (Gold et al., in prep.).

Because abundances remain fairly constant across time with PNe, the chemical changes must come in the protoplanetary nebulae (PPN) phase. This stage is a fleeting episode in stellar evolution that lasts just a few thousand years (Hrivnak et al. 2020), nestled in between the AGB and planetary nebulae. It is characterized by very fast ($\sim$ 100 km s^{-1}) collimated outflows that interact with the slower AGB wind, likely causing shocks and elevated temperatures (e.g. Lorenzo et al. 2021). In addition, the central star is beginning to evolve towards a white dwarf and emit UV radiation, causing photoionization. These conditions alter the AGB molecular content. There have been several in-depth studies of the molecular content of PPNe, most notably the C-rich objects CRL 2688 and CRL 618 (e.g. Qiu et al. 2022; Zhang et al. 2013; Pardo *et al.* 2007). Abundances of certain molecules do change from the AGB stage. For example, Zhang et al. found that both CS and HCN had lower abundances in CRL 2688 than IRC+10216 by a factor of 15. HNC becomes more prevalent with [HCN]/[HNC] $\sim$ 1 in CRL 2688 and CRL 618 (Zhang et al. 2013; Herpin & Cernicharo 2000). Molecular inventories are also being assembled for O-rich PPNe such as M1-92 and the Cotton Candy Nebula (e.g. Gold et al., in prep). Other, less well-studied objects such as IRAS Z02229+6208 also appear to have interesting chemistries (Figure 10). As a larger statistical sample is obtained for PPNe, a clearer picture of the chemical transformation will emerge for comparison with PNe.

10. A Few Comments on Dust

Both silicates and carbonaceous dust grains have been found in PNe. They are thought to reflect the grain composition formed in the AGB phase. A summary of observed dust features is given in Table 4. Common grain composition includes aromatic and aliphatic carbon dust, and amorphous and crystalline silicates (e.g. Kwok 2022). Also, in certain cases, PNe show a mixed dust grain composition, or no dust features at all (e.g. García-Hernández & Górny 2014). Surprisingly, the SiC dust feature that is almost ubiquitous in C-rich circumstellar shells is absent in PNe (Chen et al. 2022). Thus far there has been no systematic comparison of dust types and molecular composition. Perhaps of even more interest is the presence of the fullerenes C_{60} and C_{70} in certain PNe and PPNe (e.g. Zhang et al. 2016; Cami et al. 2010). The formation of these large molecules composed

https://doi.org/10.1017/S1743921324000358 Published online by Cambridge University Press

Table 4. Common Dust Features in PNe.

Feature	Wavelength (μm)
Aromatic carbon	3.3, 6.2, 7.7, 8.6, 11.3
Aliphatic carbon	3.4
Amorphous silicates	9.7, 17
Crystalline silicates	19, 24, 28, 34

of pure carbon is difficult to explain. Their origin has been attributed to PAHs and HACs (Berné & Tielens 2012). More recently, experimental work has suggested that the fullerenes arise from the destruction of SiC grains, commonly produced in circumstellar shells (Bernal et al. 2022, 2019). Shock heating of the grains leaches the silicon from the surface, creating graphitic layers that can deform into spherical structures. Nanotubes are also formed, suggesting that they may be present in the ISM.

11. Perspectives

The past decade of molecular observations of planetary nebulae have demonstrated that many of these objects are rich in gas-phase molecules, despite the presence of strong UV radiation. The molecules are present in warm, dense gas, and appear to survive in self-shielding clumps. These molecules likely represent remnant AGB material, but with abundances becoming modified in the PPN stage. Once the PN stage is attained, abundances appear to be "frozen" throughout the nebular lifetime. Therefore, the PN ejecta that populate the diffuse ISM may be in part molecular in nature, and can account for the chemistry in diffuse clouds. This molecular material also appears to play an important role in the shaping of PNe. The extreme ^{13}C enrichment observed in some PNe may additionally hold clues to unknown processes in AGB nucleosynthesis that may help shape these fascinating objects as well.

12. Acknowledgements

This work was supported by NSF Grants AST-1907910 and AST-2307305. We also thank Katherine Gold for her help and contributions of data in preparation.

References

Aaquist, O.B., & Kwok, S. 1990, *A&AS*, 84, 229
Abia, C., Hedrosa, R.P., Domínguez, I., & Straniero, O. 2017, *A&A*, 599, A39. doi:10.1051/0004-6361/201629969
Akras, S., Gonçalves, D.R., & Ramos-Larios, G. 2017, MNRAS, 465, 1289. doi:10.1093/mnras/stw2736
Andriantsaralaza, M., Zijlstra, A., & Avison, A. 2020, MNRAS, 491, 758. doi:10.1093/mnras/stz3026
Audouze, J., Truran, J.W., & Zimmerman, B.A. 1973, *ApJ*, 184, 493. doi:10.1086/152346
Bachiller, R., Forveille, T., Huggins, P.J., & Cox, P. 1997, *A&A*, 324, 1123
Balick, B., & Frank, A. 2002, *ARA&A*, 40, 439. doi:10.1146/annurev.astro.40.060401.093849
Balser, D.S., McMullin, J.P., & Wilson, T.L. 2002, *ApJ*, 572, 326. doi:10.1086/340309
Bernal, J.J., Haenecour, P., Howe, J., et al. 2019, *ApJL*, 883, L43. doi:10.3847/2041-8213/ab4206
Bernal, J.J., Zega, T.J., & Ziurys, L.M. 2022, *J. Phys. Chem.*, 126, 5761. doi:10.1021/acs.jpca.2c01441
Bernard-Salas, J., Pottasch, S. R., Feibellman, W. A., & Wesselius, P. R. 2002, A&A, 387, 301. doi:10.1051/0004-6361:2002035
Berné, O., & Tielens, A.G.G.M. 2012, *PNAS*, 109, 401, doi:10.1073/pnas.1114207108
Bublitz, J., Kastner, J.H., Hily-Blant, P., et al. 2020, *Galaxies*, 8, 32. doi:10.3390/galaxies8020032

https://doi.org/10.1017/S1743921324000358 Published online by Cambridge University Press

Bublitz, J., Kastner, J.H., Hily-Blant, P., et al. 2023, *ApJ*, 942, 14. doi:10.3847/1538-4357/aca405
Bublitz, J., Kastner, J.H., Santander-García, M., et al. 2019, *A&A*, 625, A101. doi:10.1051/0004-6361/201834408
Cami, J., Bernard-Salas, J., Peeters, E., & Malek, S.E. 2010, *Sci*, 329, 1180. doi:10.1126/science.1192035
Chen, T., Xiao, C.Y., Li, A., & Zhou, C.T. 2022, *MNRAS*, 509, 5231. doi:10.1093/mnras/stab3175
Corradi, R.L.M., Gonçalves, D.R., Villaver, E., et al. 2000, *ApJ*, 535, 823. doi:10.1086/308877
Cox, P., Omont, A., Huggins, P.J., Bachiller, R., & Forveille, T. 1992, *A&A*, 266, 420
Davis, C.J., Smith, M.D., Stern, L., Kerr, T.H., & Chiar, J.E. 2003, *MNRAS*, 344, 262. doi:10.1046/j.1365-8711.2003.06820.x
Dorschner, J., & Henning, T. 1995, *A&ARv*, 6, 271. doi: 10.1007/BF00873686
Edwards, J.L., Cox, E.G., & Ziurys, L.M. 2014, *ApJ*, 791, 79. doi:10.1088/0004-637X/791/2/79

Edwards, J.L., & Ziurys, L.M. 2013, *ApJL*, 770, L5. doi:10.1088/2041-8205/770/1/L5
Edwards, J.L., & Ziurys, L.M. 2014, *ApJL*, 794, L27. doi:10.1088/2041-8205/794/2/L27
García-Hernández, D.A., & Górny, S.K. 2014, *A&A*, 567, A12. doi:10.1051/0004-6361/201423620

Güsten, R., Wiesemeyer, H., Neufeld, D., et al. 2019, *Natur*, 568, 357. doi:10.1038/s41586-019-1090-x
Henry, R.B.C., Kwitter, K.B., & Balick, B. 2004, *AJ*, 127, 2284. doi:10.1086/382242
Henry, R.B.C., Kwitter, K.B., & Dufour, R.J. 1999, *ApJ*, 517, 782. doi:10.1086/307215
Henry, R.B.C., Stephenson, B.G., Miller Bertolami, M.M., Kwitter, K.B., & Balick, B. 2018, MNRAS, 473, 241. doi:10.1093/mnras/stx2286
Herpin, F., & Cernicharo, J. 2000, *ApJ*, 530, L129. doi:10.1086/312507
Herwig, F. 2005, *ARA&A*, 43, 435. doi:10.1146/annurev.astro.43.072103.150600
Howe, D.A., Hartquist, T.W., & Williams, D.A. 1994, *MNRAS*, 271, 811.
Hrivnak, B.J., Henson, G., Hillwig, T.C., et al. 2020, *ApJ*, 901, 9. doi:10.3847/1538-4357/abad8c
Huggins, P.J., Bachiller, R., Cox, P., & Forveille, T. 1996, *A&A*, 315, 284.
Huggins, P.J., Bachiller, R., Planesas, P., Forveille, T., & Cox, P., 2005, *ApJSS*, 160, 272
Huggins, P.J., & Healy, A.P., 1989, *ApJ*, 346, 201.
Kwok, S. 2022, *FrASS*, 9, 893061. doi:10.3389/fspas.2022.893061
Lebzelter, T., Hinkle, K.H., Straniero, O., et al. 2019, *ApJ*, 886, 117. doi:10.3847/1538-4357/ab4e9b
Liu, X.-W., Barlow, M.J., & Cohen, M. 2001, MNRAS, 323, 343. doi:10.1046/j.1365-8711.2001.04180.x
López-Martín, L., López, J.A., Esteban, C., et al. 2002, *A&A*, 388, 652. doi:10.1051/0004-6361:20020502
Lorenzo, M., Teyssier, D., Bujarrabal, V., et al. 2021, *A&A*, 649, A164. doi:10.1051/0004-6361/202039592
Marquez-Lugo, R.A., Ramos-Larios, G., Guerrero, M.A., & Vázquez, R. 2013, 429, 973. doi:10.1093/mnras/sts381
Meixner, M., McCullough, P., Hartman, J., Son, M., & Speck, A. 2005, *AJ*, 130, 1784. doi:10.1086/444539
Milam, S.N., Woolf, N.J., & Ziurys, L.M. 2009, *ApJ*, 690, 837. doi:10.1088/0004-637X/690/1/837
Moraga Baez, P., Kastner, J.H., Balick, B., Montez, Jr., R., & Bublitz, J. 2023, ApJ, 942, 15. doi:10.3847/1538-4357/aca401
Neufeld, D.A., Goto, Miwa, Geballe, T.R., et al. 2020, 894, 37. doi:10.3847/1538-4357/ab7191
Palla, F., Bachiller, R., Stanghellini, L., Tosi, M., & Galli, D. 2000, *A&A*, 355, 69.
Pardo, J.R., Cernicharo, J., Goicoechea, J.R., Guélin, M., Asensio Ramos, A. 2007, *ApJ*, 661, 250. doi:10.1086/513734

https://doi.org/10.1017/S1743921324000358 Published online by Cambridge University Press

Pottasch, S.R., Beintema, D.A., & Feibelman, W.A. 2000, *A&A*, 363, 767
Pulliam, R.L., Edwards, J.L., & Ziurys, L.M. 2011, *ApJ*, 743, 36. doi:10.1088/0004-637X/743/1/36
Qiu, J.-J., Zhang, Y., Zhang, J.-S., & Nakashima, J. 2022, *ApJS*, 259, 56. doi:10.3847/1538-4365/ac5180
Ramstedt, S., & Olofsson, H. 2014, *A&A*, 566, A145. doi:10.1051/0004-6361/201423721
Redman, M.P., Viti, S., Cau, P., & Williams, D.A., 2003, *MNRAS*, 345, 1291. doi:10.1046/j.1365-2966.2003.07047.x
Sahai, R., Vlemmings, W.H.T., Huggins, P.J., & Nyman, L.-Å. 2017, *ApJ*, 841, 110. doi:10.3847/1538-4357/aa6d86
Sahai, R., Vlemmings, W.H.T., Huggins, P.J., Nyman, L.-Å, & Gonidakis, I. 2013, *ApJ*, 777, 92. doi:10.1088/0004-637X/777/2/92
Schmidt, D.R., Gold, K.R., Sinclair, A., Bergstrom, S., & Ziurys, L.M. 2022, *ApJ*, 927, 46. doi:10.3847/1538-4357/ac4474
Schmidt, D.R., Woolf, N.J., Zega, T.J., & Ziurys, L.M. 2018b, *Natur*, 564, 378. doi:10.1038/s41586-018-0763-1
Schmidt, D.R., Zack, L.N., & Ziurys, L.M. 2018a, *ApJL*, 864, L31. doi:10.3847/2041-8213/aadc09
Schmidt, D.R., & Ziurys, L.M. 2016, *ApJ*, 817, 175. doi:10.3847/0004-637X/817/2/175
Schmidt, D.R., & Ziurys, L.M. 2017a, *ApJ*, 835, 79. doi:10.3847/1538-4357/835/1/79
Schmidt, D.R., & Ziurys, L.M. 2017b, *ApJ*, 850, 123. doi:10.3847/1538-4357/aa8a6a
Schmidt, D.R., & Ziurys, L.M. 2019, *ApJL*, 881, L38. doi:10.3847/2041-8213/ab3663
Snow, T.P., & McCall, B.J. 2006, *ARA&A*, 44, 367. doi:10.1146/annurev.astro.43.072103.150624
Speck, A.K., Meixner, M., Jacoby, G.H., & Knezek, P.M. 2003, *PASP*, 115, 170. doi:10.1086/345911
Tenenbaum, E.D., Milam, S.N., Woolf, N.J., & Ziurys, L.M. 2009, *ApJ*, 704, L108. doi:10.1088/0004-637X/704/2/L108
Ventura, P., Stanghellini, L., Dell'Agli, F., & García-Hernández, D.A., 2017, MNRAS, 471, 4648. doi:10.1093/mnras/stx1907
Weidmann, W.A., & Gamen, R. 2011, *A&A*, 526, A6. doi:10.1051/0004-6361/200913984
Wiescher, M., Görres, J., Uberseder, E., Imbriani, G., & Pignatari, M. 2010, *Ann. Rev. Nucl. Part. Sci.*, 60, 381. doi:10.1146/annurev.nucl.012809.104505
Zack, L.N., & Ziurys, L.M. 2013, *ApJ*, 765, 112. doi:10.1088/0004-637X/765/2/112
Zeigler, N.R., Zack, L.N., Woolf, N.J., & Ziurys, L.M., 2013, *ApJ*, 778, 16. doi:10.1008/0004-637X/778/1/
Zhang, Y., Kwok, S., & Dinh-V-Trung 2008, *ApJ*, 678, 328. doi:10.1086/529428
Zhang, Y., Kwok, S., Nakashima, J., Chau, W., & Trung, D.-V. 2013, *ApJ*, 773, 71. doi:10.1088/0004-637X/773/1/71
Zhang, Y., Kwok, S., & Sadjadi, S. 2016, *JPhCS*, 728, e052004. doi:10.1088/1742-6596/728/5/052004
Ziurys, L.M., Schmidt, D.R., & Woolf, N.J. 2020, *ApJL*, 900, L31. doi:10.3847/2041-8213/abb082
Ziurys, L.M., Tenenbaum, E.D., Pulliam, R.L., Woolf, N.J., & Milam, S.N. 2009, *ApJ*, 695, 1604. doi:10.1088/0004-637X/695/2/1604

https://doi.org/10.1017/S1743921324000358 Published online by Cambridge University Press